TiO2@CeOx Core−Shell Nanoparticles as Artificial Enzymes with Peroxidase-Like Activity

Luca Artiglia, Stefano Agnoli, Maria Cristina Paganini, Mattia Cattelan, and Gaetano Granozzi
TiO2@CeOx Core?Shell Nanoparticles as Artificial Enzymes withPeroxidase-Like Activity
ACS APPLIED MATERIALS & INTERFACES (2014) 6
DOI: 10.1021/am5057129

TiO_2@CeO_x Core-Shell Nanoparticles as Artificial Enzymes with Peroxidase-Like Activity

Luca Artiglia,[#] Stefano Agnoli,[#] Maria Cristina Paganini,[§] Gaetano Granozzi[#]*

[#]Department of Chemical Sciences, University of Padova, via Marzolo 1, I-35131 Padova, Italy

[§]Department of Chemistry, University of Torino, via Giuria 7 – 10125 Torino, Italy

Keywords: Titanium dioxide. Cerium oxide. Interface hybridization. Core-shell. Artificial Enzyme. Peroxidase.

ABSTRACT

The $Ce^{4+} \leftrightarrow Ce^{3+}$ redox switch is at the basis of an all-inorganic catalytic cycle that is capable to mimic the activity of several natural redox enzymes. The efficiency of these artificial enzymes (nanozymes) strongly depends on the Ce^{4+}/Ce^{3+} ratio. By capitalizing on the results obtained on oxide/oxide model systems, we implemented a simple and effective procedure to obtain conformal TiO_2@CeO_x core-shell nanoparticles whose thickness is controlled with single layer precision. Since the Ce^{3+} species are stabilized only at the interface by the electronic hybridization with the TiO_2 states, the modulation of the shell thickness offers a simple method to tailor the Ce^{4+}/Ce^{3+} ratio and therefore the catalytic properties. The activity of these nanoparticles as artificial peroxidase-like enzymes was tested, showing exceptional

performances, even better than natural horseradish peroxidase enzyme. The main advantage with respect to other oxide/oxide nanozymes is that our nanoparticles, having a tunable Ce^{4+}/Ce^{3+} ratio, are efficient already at low H_2O_2 concentrations.

INTRODUCTION

Cerium oxide, CeO_2, is one of the most interesting oxides in catalysis, being an efficient catalyst itself or a subtle structural and electronic promoter in several chemical processes.[1,2,3,4,5] The key point at the basis of its catalytic activity is the low energy cost for the formation of oxygen vacancies and Ce^{3+} centers. Since these chemical species are extremely catalytically active, a huge amount of studies have focused on the strategies to maximize their amount, stability and organization. Among the several processes that are controlled by ceria defects, the oxygen activation is maybe the most important since it impacts very different chemical fields, such as high yield industrial reactions, fine chemical and even biological syntheses.[6,7,8] Actually, the $Ce^{4+}\leftrightarrow Ce^{3+}$ redox switch is the all-inorganic analogue of the catalytic cycle of redox enzymes[9,10,11,12,13] where metal centers are used as co-factors to promote reversible redox reactions and/or against intracellular oxidative stress[14,15,16] in cell metabolism.

So far, several strategies have been used to manipulate the Ce^{4+}/Ce^{3+} ratio, such as reduction in the geometrical size,[17,18] introduction of dopants or other oxides and kinetically controlled synthesis.[19,20,21,22] The outcomes of these works have demonstrated that the presence of defects enhances significantly the reactivity, although in many cases, defects are metastable and their chemical activity is lost as a consequence of NPs coalescence and/or interaction with the reaction environment.

In this paper we propose a radically new approach, based on the creation of an oxide/oxide interface capable to provide a strong stabilization for defect centers. Following the blueprint outlined from theoretical[23] and experimental model studies,[24] it emerges the possibility of stabilizing Ce^{3+} by the interfacial hybridization with a reducible oxide support. In the case of titania, by virtue of the electronic hybridization between the TiO_2 O 2*p* band and Ce 4*f* states, Ce^{3+} species are strongly stabilized with respect to unsupported ceria, allowing to obtain almost exclusively reduced species at the interface in a wide range of experimental conditions.[23,25,26] Interestingly, the localized nature of electronic hybridization determines that the stabilization of reduced states is sensibly thickness dependent. Recently, it has been demonstrated that when the CeO_x coverage exceeds the monolayer, the interface hybridization is progressively lost, so that stoichiometric CeO_2 starts to grow.[24] This opens the way to the control of the Ce^{4+}/Ce^{3+} ratio simply by choosing the thickness of the ceria shell supported on TiO_2.

Taking the cue from this vision, in the following work we optimized a synthetic protocol based on atomic layer deposition of an organometallic Ce^{3+} precursor on a commercial TiO_2 powder suspension, with the aim of obtaining a of single layer of CeO_x on TiO_2, and therefore preparing thickness controlled $TiO_2@CeO_x$ core-shell nanoparticles (NPs). The activity as a peroxidase-like enzyme of core-shell NPs with different Ce^{4+}/Ce^{3+} ratios has been tested by means of a biomimetic assay.

The success of this synthesis scheme indicates that the use of core-shell nanoparticles bearing controlled interfaces represents a suitable approach for the realization of nanostructures with specific functionalities. Actually, with respect to standard nanoparticles (e.g. simple nanoceria), core–shell systems can be designed in order to combine the bulk properties of the core (e.g. magnetism, light adsorption or emission) with very specific chemical properties of

the shell, so that the resulting system can explicate multiple functions.[27,28] Moreover the strong electronic stabilization intrinsic to the formation of the oxide/oxide interface provides an effective strategy to promote biocompatibility, and to enhance chemical stability in harsh conditions.

MATERIALS AND METHODS

Synthesis of the TiO_2@CeO_x core-shell NPs

The core-shell samples have been obtained by impregnation of a commercial TiO_2 powder (Degussa Aeroxide© P25) in a Cerium (III) 2-ethylhexanoate (49% in 2-ethylhexanoic acid, Alfa Aesar) precursor solution.[29] The TiO_2 powder was pre-treated at 570 K in air to remove any water residual and then added to a 0.75 mol/L solution of the precursor in n-hexane at room temperature (thermostatic bath). The mixture was stirred for 5 hours, afterwards the powder was filtered and washed with n-hexane to remove any precursor residue. The product was dried and then calcined at 920 K (heating ramp of 5 K/min) in air for 8 hours.

Structural and functional characterization

Transmission electron microscopy (TEM) analysis of the powder samples deposited on a copper grid was performed in Torino, using a Jeol JEM 3010 (300 kV) microscope equipped with an EDS detector by Oxford Instruments.

X ray photoelectron spectroscopy (XPS) spectra were collected in Padova in a Ultra High Vacuum chamber (base pressure 1.0×10^{-9} mbar) equipped with a VG MKII Escalab electron analyzer. Photoemission spectra were taken at room temperature in normal emission using a non-monochromatized Al anode X-ray source (hv=1486.6 eV). Powder samples were

suspended in bi-distilled water and drop casted on high purity copper foils. After drying in air the obtained films were introduced into the ultrahigh vacuum chamber and outgassed overnight. The charging observed during measurements was corrected using adventitious carbon as the internal reference.

For peroxidase-like kinetic assays, 3,3',5,5'-Tetramethylbenzidine (TMB) was purchased from Sigma Aldrich. All the tests were performed in a pH=4 citrate buffer using different concentrations of either TMB or H_2O_2 (35%, Sigma Aldrich) and 200 µg/mL of TC samples powder.

The peroxidase-like reaction, catalyzed by TC powders, is the following:

$$TMB(aq) + H_2O_2(aq) \rightarrow oxTMB(aq) + 2H_2O(l)$$

This reaction follows a ping-pong mechanism, in which 3,3',5,5'-tetramethybenzidine (TMB, transparent solution) is oxidized to 3,3',5,5'-tetramethylbenzidine diimine (oxTMB, blue solution) and H_2O_2 is reduced to H_2O.

As long as the reaction proceeds and TMB is oxidized to oxTMB, the solution turns to blue (see Figure S1), thus the kinetics can be monitored acquiring the oxTMB absorbance peak, centered at λ=652 nm. The UV-Vis spectra were collected at 120 seconds steps in a Varian Cary-50 spectrometer, with a scan rate of 600 nm/min.

RESULTS AND DISCUSSION

Synthesis and characterization of core-shell NPs

CeO_x nanostructures, where Ce^{3+} species are stabilized by the interaction with the substrate, were grown on TiO_2 in ideal conditions (ultra high vacuum) by physical vapor deposition of a controlled amount of metallic Ce (electron beam evaporation from a metallic Ce target) in controlled oxygen environments, followed by thermal treatment.[24] Nevertheless, a simpler and highly scalable synthetic route, characterized by the same level accuracy in the shell thickness, can be followed by taking advantage of the surface hydroxyl species on the TiO_2 support, which can be exploited to promote a surface sol-gel reaction with the Ce organometallic precursor. This reaction eventually leads to a Ti-O-Ce-$(OR)_x$ layer, whose organic component is removed during the calcination. Cerium (III) 2-ethylhexanoate was chosen due to the steric protection of the metallic center and the reaction was carried out in anhydrous conditions (anhydrous n-hexane solvent) to avoid any Ce^{3+} oxidation during the impregnation. In the following we will discuss the behavior of two samples obtained after:

i) a single impregnation (5 hours in 0.75 mol/L n-hexane solution of the Ce precursor) + calcination (8 hours at 920 K in air) step (named **TC1**);

ii) three consecutive impregnation steps (5 hours in 0.75 mol/L n-hexane solution of the Ce precursor) + calcination (8 hours at 920 K in air) steps (named **TC3**).

We report the TEM images of TC1 and TC3 in Figure 1a,b, respectively. In the former case, it is possible to observe the typical TiO_2 crystal shape, whose edges are outlined by a very thin darker border due to the presence of ceria, as confirmed by EDX measurements (see SI, Table S1).

By repeating three times the impregnation + calcination procedure (TC3), a thicker layer (1-1.5 nm i.e. ca 3 ML) of amorphous ceria covers conformally the titania nanocrystals, evidencing a layer by layer growth mode. Lower magnification TEM images (100000x) of TC1 and TC3 are reported in figure S2 and S3, respectively. Figure 32 demonstrates that all

the NPs are uniformly covered by the CeO_x shell. An evaluation of the NPs average dimension has given 22.8±0.3 nm for TC1 and 25.9±0.9 nm for TC3. Such an increase could be due to the multiple heating treatments at 920 K performed on the latter.

XPS data of the Ce 3*d* core levels are displayed in Figure 2. The photoemission spectrum of a CeO_2 nanopowder, taken as a reference (see Figure S3 in SI), shows the three typical spin-orbit-split doublets corresponding to the different 4*f* configurations in the photoemission final state.[24,30] The component labeled u^{iii} at 916.3 eV is indicative of the poorly screened Ce $3d^9 4f^0$ O $2p^6$ final state, connected with the presence of Ce^{4+} ions. The XPS data of TC1 and TC3 strongly differ from the reference CeO_2. The former, (Figure 2a), shows only two peaks at 881.1 and 885.0 eV (labelled as v^0 and v^i, respectively), replicated by spin-orbit-splitting satellites (18.2 eV), which can be ascribed to Ce $3d^9 4f^2$ O $2p^5$ and Ce $3d^9 4f^1$ O $2p^6$ final states, respectively. These findings, combined with the absence of the u^{iii} peak, reveal the almost exclusive presence of Ce^{3+} ions, confirming that one monolayer of ceria is stabilized in the reduced state by the interaction with TiO_2. On the contrary, the XPS data corresponding to TC3 (Figure 2c) differs from TC1, showing a change in the relative intensity between the different components and the presence of the u^{iii} satellite. Therefore, the TC3 XPS data are representative of an oxide whose composition is an "average" between stoichiometric CeO_2 and TC1. A multipeak analysis of the 3*d* photoemission peaks (Figure 2c) allows a quantification of the Ce^{3+} (v^0, v^i) and Ce^{4+} (v, v^{ii}, v^{iii}) components (72% Ce^{3+} and 28% Ce^{4+}). Thence, TC3 is a TiO_2@CeO_x core-shell where Ce^{3+} ions, stabilized at the interface with TiO_2, and fully oxidized Ce^{4+} ions are co-present. Moreover, the stabilization of Ce^{3+} species does not depend on extrinsic factors, such as nanodimension or metastable state obtained during a kinetically driven synthesis, but on an electronic interaction that is unaffected by ambient conditions.

Reactivity of core-shell NPs as artificial enzymes

Being able to synthesize ceria coated NPs characterized by a tunable amount of Ce^{4+}/Ce^{3+} but identical in terms of structure, morphology, dimensions and surface area, we decided to investigate how defectivity impacts on their activity as artificial enzymes. Recently, ceria NPs with different Ce^{4+}/Ce^{3+} ratios showed the ability to act as mimics of superoxide dismutase, catalase and oxidase, thus proving to be efficient artificial enzymes (often referenced as nanozymes)[31] able to protect cells from the oxidative stress due to an excess of reactive oxygen species.[9,10,11,12,13,32,33] In a recent work, Peng et al.[33] asserted that CeO_2 NPs, instead of working as a catalyst, behave as an oxidizing agent, due to the progressive dissolution of Ce^{3+} in the reactive mixture. Therefore, a good strategy to prevent this leaching is to stabilize the Ce^{3+} active sites, allowing CeO_x to run like a catalyst.

As a case study, we investigated the activity of $TiO_2@CeO_x$ as a peroxidase-like enzyme using standard colorimetric tests based on 3,3',5,5'-Tetramethylbenzidine (TMB) oxidation. Similarly to the horseradish peroxidase (HRP) natural enzyme, CeO_2 NP catalytic activity is dependent on the pH, temperature and concentration of H_2O_2. In agreement with previous biomimetic assays, our tests were performed at 300 K and pH=4.0 buffer.[13,33] Figures 3a and 3b show the reaction rate for TC1 and TC3 as a function of the H_2O_2 substrate, obtained at a fixed TMB concentration (0.2 mM). The reaction rate calculated using TMB as a substrate ($[H_2O_2]$=0.058 M) is reported for both samples in Figure 3c.

Based on the data reported in Figure 3, in a wide range of TMB and H_2O_2 concentrations we could obtain the apparent Michaelis-Menten steady-state kinetic parameters to evaluate the peroxidase-like activity. The results (double reciprocal plots) are shown in Figure S4. The first tests, obtained adding variable amount of TMB to a solution of $[H_2O_2]$ at fixed concentration (0.058 M), show that TC1 and TC3 kinetic parameters are comparable

(K_M^{app}=0.28 and 0.30 mM, respectively, see Table 1), but lower with respect to HRP (0.43 mM),[34] denoting a good affinity for TMB, which is a common feature of all inorganic mimics of peroxidase, such as Fe_3O_4,[34] CuO,[35] and FeS.[36,37] On the contrary, the affinity towards the oxidant is much scarcer. In general, nanozymes require a higher peroxide concentration than HRP to reach the maximum activity.[34,35,38] Interestingly, our core-shell NPs escape this trend. As a matter of fact, if H_2O_2 is tested as a substrate, by changing its concentration in the presence of 0.2 mM TMB the TC1 K_M^{app} value increases by about 20 times and its calculated value (6.29 mM) is higher than that measured for HRP,[34] however order of magnitude smaller than other oxides (CuO 85.6 mM, Fe_3O_4 154 mM, see Table 1)[34,35] and comparable with other highly efficient mimics (graphene oxide 3.99 mM, FeS 7.2 mM).[36,38] Surprisingly, also TC3 shows an increase of the K_M^{app} (1.39 mM), but quite modest, smaller than the natural enzyme.

Therefore, the apparent kinetic parameters point out an exceptional performance for TC1 and especially for TC3 samples as peroxidase-like enzymes, showing a strong affinity for TMB and, above all, for the oxidant molecule H_2O_2. This result is of paramount importance since the main limit of inorganic mimics is their need for high concentration of H_2O_2 in order to work efficiently, which prevents their application in sensitive environments.[34,35] To rationalize the differences observed in the catalytic activity, we acquired the Ce 3*d* photoemission lines after the reaction of the TC samples with a 0.058 M solution of H_2O_2 (i. e. the same concentration used in the biomimetic assays). The resulting spectra (Figure 2b,d) show that both samples undergo a modification, due to the presence/increase of Ce^{4+} peaks after the reaction with the H_2O_2 solution. In particular, the multipeak analysis demonstrates that the relative percentage of the Ce^{4+} peaks (that is the sum of the v, v^{ii} and v^{iii} multiplet/total Ce 3*d* area) passes from 0% to 50% for TC1 and from 28% to 91% for TC3, indicating that TC3 is more prone to oxidation than TC1.

Therefore, if we assume a ping-pong mechanism for the TMB oxidation,[34] where initially the Ce^{3+}centres react with H_2O_2 with a consequent oxidation to Ce^{4+}, the lower affinity of the TC1 toward the H_2O_2 substrate can be traced back to an excessive stabilization of Ce^{3+} sites at the interface with TiO_2, which hinders the redox switching of the Ce^{4+}/Ce^{3+} couple. Interestingly, the interfacial stabilization operated by TiO_2 not only changes quantitatively the Ce^{4+}/Ce^{3+} ratio, but also the very tendency of the reduced species to be oxidized.

CONCLUSION

Our results describe a procedure to obtain $TiO_2@CeO_x$ NPs by a simple and well reproducible impregnation technique. In this way it is possible to tune the thickness of the CeO_x shell and, by doing so, its oxidation state. In fact, in agreement with works on model systems,[24] Ce^{3+} ions are stabilized at the interface with TiO_2 and, as long as the shell thickness is increased, it is possible to increase the Ce^{4+}/Ce^{3+} ratio. The electron shuttling between defects states (i.e. Ti 3*d* and Ce 4*f* bands) in heterointerfaces has demonstrated to be a totally general phenomenon[39,40,41] that can be extended to other reducible oxides, in order to stabilize active chemical species. This paves the way to a full gamut of core-shell nanoparticles characterized by enhanced chemical activity but that can also benefit form the intrinsic bulk properties of the core, which can be magnetic or optically active in order to implement in a single nanosystem multiple functionalities.

The activity of $TiO_2@CeO_x$ as a peroxidase-like enzyme was tested by a colorimetric method employing TMB and H_2O_2. The apparent Michaelis-Menten kinetic parameters revealed that the shell thickness has a role in the catalyst activity. The TC3 sample showed the best performances (in line or better than the natural HRP enzyme), i.e. good affinity for TMB and, above all, for H_2O_2. Moreover, we demonstrated that the large hybridization between TiO_2

and CeO_x in TC1 stabilizes exclusively Ce^{3+} at the interface, hindering its oxidation to Ce^{4+}. On the contrary, a 30%/70% ratio between Ce^{4+} and Ce^{3+} ions (TC3) promotes Ce^{3+} oxidation. Therefore the interface not only changes quantitatively the number or reduced species, but also the intrinsic tendency of metal centers to accept or donates electrons. This provides a quite sophisticated and very general method to tune the redox switch of a catalytic cycle and to bring it in the conditions where the activity is maximized.[42,43]

FIGURES

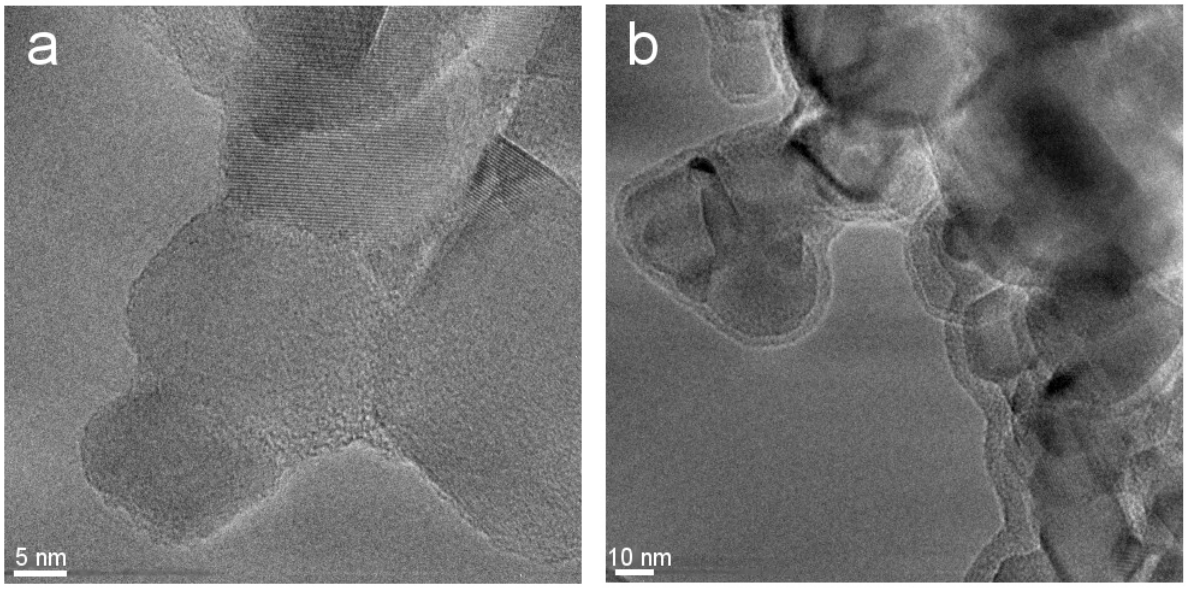

Figure 1. TEM Images of TiO_2@CeO_x samples: a) TC1 (400000x) and b) TC3 (150000x). The conformal growth of ceria, indicative of a layer-by-layer growth is evident from the huge homogeneity and perfectly wetting behavior of the outer shell surrounding the TiO_2nanocrystals.

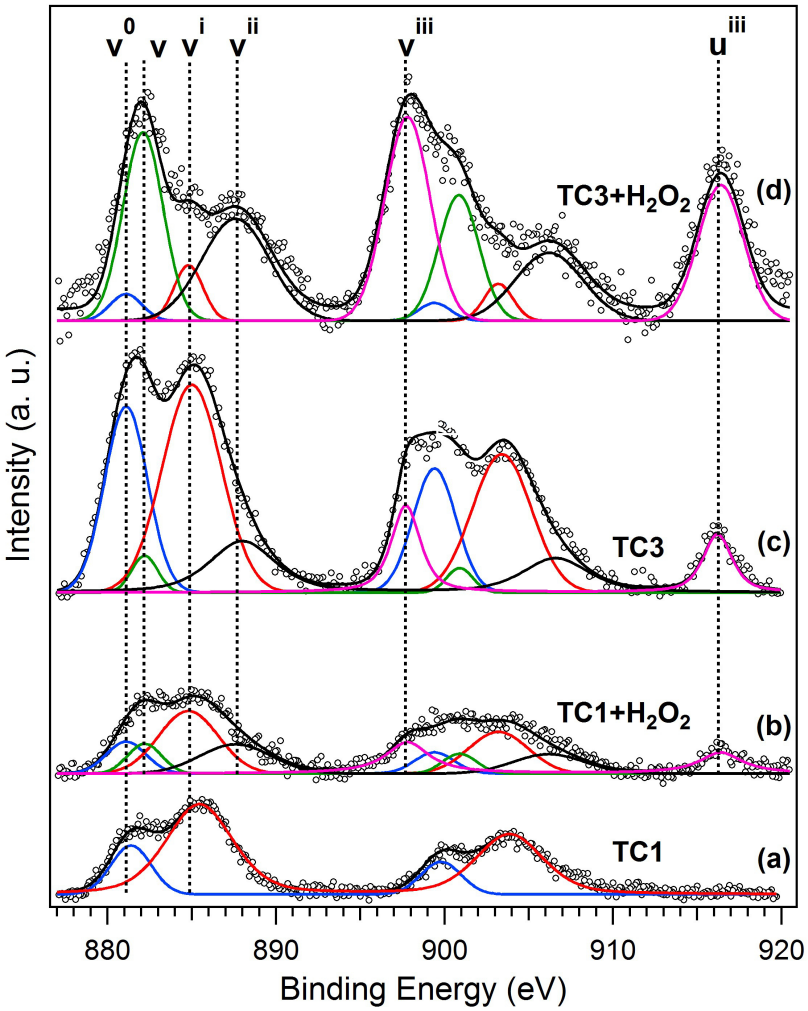

Figure 2. XPS Ce 3d data of the TiO_2@CeO_x powders obtained after calcination, (a) TC1, (c) TC3, and after reaction in a 0.058 M H_2O_2 solution, (b) TC1, (d) TC3.

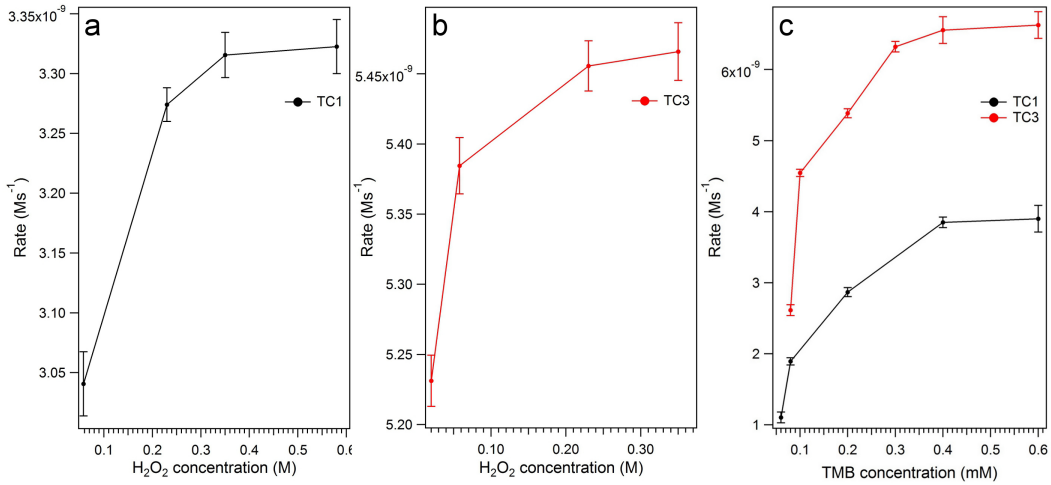

Figure 3. Reaction rate of TC1 (a) and TC3 (b) samples at different [H_2O_2] ([TMB]=0.2 mM) and (c) reaction rate of TC samples as a function of [TMB] ([H_2O_2]=0.058 M)

TABLES

Table 1. Apparent kinetic parameters obtained from the double reciprocal plots (see Figure S3) compared with the natural enzyme (HRP) and other artificial enzymes.

Catalyst+ Substrate	**K_M^{app} [mM]**	**V_{MAX}^{app} [nMs^{-1}]**
TC1 + TMB	0.28±0.03	6.5±0.3
TC1 + H_2O_2	6.29±0.94	34.0±3.0
TC3 + TMB	0.30±0.04	12.0±0.6
TC3 + H_2O_2	1.39±0.15	55±5.0
HRP[34]+TMB	0.434	10.0
HRP[34]+ H_2O_2	3.70	87.0
CuO[35]+TMB	0.013	NA
CuO[35]+H_2O_2	85.6	NA
Fe_3O_4[34]+TMB	0.098	34.4
Fe_3O_4[34]+H_2O_2	154	97.8
GO-COOH[38] + TMB	0.0237± 0.001	34.5±3.1
GO-COOH[38]+H_2O_2	3.99±0.67	38.5±2.2
FeS[36]+TMB	0.13	NA
FeS[36]+H_2O_2	7.2	NA

ASSOCIATED CONTENT

Supporting Information

Additional TEM micrographs, with relative statistical analysis, photoemission spectra and details about enzyme assays (double reciprocal plots) are provided. This material is available free of charge via the Internet at http://pubs.acs.org.

AUTHOR INFORMATION

Corresponding Author

E-mail: stefano.agnoli@unipd.it

ACKNOWLEDGEMENT

This work has been funded by the Italian Ministry of Instruction, University and Research (MIUR) through the FIRB Project RBAP115AYN "Oxides at the nanoscale: multifunctionality and applications". We thank prof. Paolo Scrimin for useful discussion.

REFERENCES

(1) Senanayake, S. D.; Stacchiola, D.; Rodriguez, J. A. Unique Properties of Ceria Nanoparticles Supported on Metals: Novel Inverse Ceria/Copper Catalysts for CO Oxidation and the Water-Gas Shift Reaction. *Acc. Chem. Res.* **2013**, *46*, 1702-1711.

(2) Rodriguez, J. A.; Graciani, J.; Evans, J.; Park, J. B.; Yang, F.; Stacchiola, D.; Senanayake, S. D.; Ma, S. G.; Perez, M.; Liu, P.; Sanz, J. F.; Hrbek, J. Water-Gas Shift Reaction on a Highly Active Inverse CeO_x/Cu(111) Catalyst: Unique Role of Ceria Nanoparticles. *Angew. Chem. Int. Edit.* **2009**, *48*, 8047-8050.

(3) Fu, Q.; Saltsburg, H.; Flytzani-Stephanopoulos, M. Active Nonmetallic Au and Pt Species on Ceria-Based Water-Gas Shift Catalysts. *Science* **2003**, *301*, 935-938.

(4) Bunluesin, T.; Gorte, R. J.; Graham, G. W. Studies of the water-gas-shift reaction on ceria-supported Pt, Pd, and Rh: Implications for oxygen-storage properties. *Appl. Catal. B-Environ.* **1998**, *15*, 107-114.

(5) Li, H.; Lu, G.; Dai, Q.; Wang, Y.; Guo Y.; Guo, Y. Hierarchical Organization and Catalytic Activity of High-Surface-Area Mesoporous Ceria Microspheres Prepared Via Hydrothermal Routes *ACS Appl. Mater. Interfaces*, **2010**, *2*, 838–846.

(6) Rao, G. R.; Fornasiero, P.; Di Monte, R.; Kaspar, J.; Vlaic, G.; Balducci, G.; Meriani, S.; Gubitosa, G.; Cremona, A.; Graziani, M. Reduction of NO over Partially Reduced Metal-Loaded CeO_2–ZrO_2 Solid Solutions. *J. Catal.* **1996**, *162*, 1-9.

(7) Esch, F.; Fabris, S.; Zhou, L.; Montini, T.; Africh, C.; Fornasiero, P.; Comelli, G.; Rosei, R. Electron Localization Determines Defect Formation on Ceria Substrates. *Science* **2005**, *309*, 752-755.

(8) Campbell, C. T.; Peden, C. H. F. Oxygen Vacancies and Catalysis on Ceria Surfaces. *Science* **2005**, *309*, 713-714.

(9) Karakoti, A. S.; Singh, S.; Kumar, A.; Malinska, M.; Kuchibhatla, S. V. N. T.; Wozniak, K.; Self, W. T.; Seal, S. PEGylated Nanoceria as Radical Scavenger with Tunable Redox Chemistry. *J. Am. Chem. Soc.* **2009**, *131*, 14144-14145.

(10) Pirmohamed, T.; Dowding, J. M.; Singh, S.; Wasserman, B.; Heckert, E.; Karakoti, A. S.; King, J. E. S.; Seal, S.; Self, W. T. Nanoceria exhibit redox state-dependent catalase mimetic activity. *Chem. Commun.* **2010**, *46*, 2736-2738.

(11) Korsvik, C.; Patil, S.; Seal, S.; Self, W. T. Superoxide dismutase mimetic properties exhibited by vacancy engineered ceria nanoparticles. *Chem. Commun.* **2007**, *46*, 1056-1058.

(12) Chen, J. P.; Patil, S.; Seal, S.; McGinnis, J. F. Rare earth nanoparticles prevent retinal degeneration induced by intracellular peroxides. *Nat. Nanotechnol.* **2006**, *1*, 142-150.

(13) Asati, A.; Santra, S.; Kaittanis, C.; Nath, S.; Perez, J. M. Oxidase-Like Activity of Polymer-Coated Cerium Oxide Nanoparticles. *Angew. Chem. Int. Edit.* **2009**, *48*, 2308-2312.

(13) Hirst, S. M.; Karakoti, A. S.; Tyler, R. D.; Sriranganathan, N.; Seal, S.; Reilly, C. M. Anti-inflammatory Properties of Cerium Oxide Nanoparticles. *Small* **2009**, *5*, 2848-2856.

(15) Menchón, C.; Martín, R.; Apostolova, N.; Victor, V. M.; Álvaro, M.; Herance, J. R.; García, H. Gold Nanoparticles Supported on Nanoparticulate Ceria as a Powerful Agent against Intracellular Oxidative Stress. *Small* **2008**, *8*, 1895-1903.

(16) Pinna, A.; Lasio, B.; Piccinini, M.; Marmiroli, B.; Amentisch, H.; Falcaro, P.; Tokudome, Y.; Malfatti, L.; innocenzi, P. Combining Top-Down and Bottom-Up Routes for Fabrication of Mesoporous Titania Films Containing Ceria Nanoparticles for Free Radical Scavenging *ACS Appl. Mater. Interfaces,* **2013**, *5*, 3168–3175.

(17) Sayle, T. X. T.; Parker, S. C.; Sayle, D. C. Shape of CeO_2 nanoparticles using simulated amorphisation and recrystallisation. *Chem. Commun.* **2004**, 2438-2439.

(18) Deshpande, S.; Patil, S.; Kuchibhata, S. V. N. T.; Seal, S. Size dependency variation in lattice parameter and valency states in nanocrystalline cerium oxide. *Appl. Phys. Lett.* **2005**, *87*, 133113.

(19) Cargnello, M.; Jaen, J. J. D.; Garrido, J. C. H.; Bakhmutsky, K.; Montini, T.; Gamez, J. J. C.; Gorte, R. J.; Fornasiero, P. Exceptional Activity for Methane Combustion over Modular Pd@CeO_2 Subunits on Functionalized Al_2O_3. *Science* **2012**, *337*, 713-717.

(20) Zhou, G.; Barrio, L.; Agnoli, S.; Senanayake, S. D.; Evans, J.; Kubacka, A.; Estrella, M.; Hanson, J. C.; Martinez-Arias, A.; Fernandez-Garcia, M.; Rodriguez, J. A. High Activity of $Ce_{1-x}Ni_xO_{2-y}$ for H_2 Production through Ethanol Steam Reforming: Tuning Catalytic Performance through Metal–Oxide Interactions. *Angew. Chem. Int. Edit.* **2010**, *49*, 9680-9684.

(21) Gionco, C.; Paganini, M. C.; Agnoli, S.; Reeder, A. E.; Giamello, E. Structural and spectroscopic characterization of CeO_2–TiO_2 mixed oxides. *J. Mater. Chem. A* **2013**, *1*, 10918-10926.

(22) Chen, L.; Si, Z.; Wu, X.; Wenig.; DRIFT Study of CuO–CeO_2–TiO_2 Mixed Oxides for NOx Reduction with NH3 at Low Temperatures *ACS Appl. Mater. Interfaces*, **2014**, *6*, 8134–8145.

(23) Graciani, J.; Plata, J. J.; Sanz, J. F.; Liu, P.; Rodriguez, J. A. A theoretical insight into the catalytic effect of a mixed-metal oxide at the nanometer level: The case of the highly active metal/CeO_x/TiO_2(110) catalysts. *J. Chem. Phys.* **2010**, *132*, 104703.

(24) Agnoli, S.; Reeder, A. E.; Senanayake, S. D.; Hrbek, J.; Rodriguez, J. A. Structure and special chemical reactivity of interface-stabilized cerium oxide nanolayers on TiO_2(110). *Nanoscale* **2014**, *6*, 800-810.

(25) Park, J. B.; Graciani, J.; Evans, J.; Stacchiola, D.; Ma, S. G.; Liu, P.; Nambu, A.; Sanz, J. F.; Hrbek, J.; Rodriguez, J. A. High catalytic activity of Au/CeO_x/TiO_2(110) controlled by the nature of the mixed-metal oxide at the nanometer level. *Proc. Natl. Acad. Sci. USA* **2009**, *106*, 4975-4980.

(26) Abbott, H. L.; Uhl, A.; Baron, M.; Lei, Y.; Meyer, R. J.; Stacchiola, D.; Bondarchuk, O.; Shaikhutdinov, S.; Freund, H. J. Relating methanol oxidation to the structure of ceria-supported vanadia monolayer catalysts. *J. Catal.* **2010**, *272*, 82-91.

(27) Wei, S.; Wang, Q.; Zhu, J.; Sun, L.; Line, H.; Guo, Z. Multifunctional composite core–shell nanoparticlesNanoscale, **2011**, 3, 4474-4502.

(28) Gao, J.; Gu, H.; Xu, B.; Multifunctional Magnetic Nanoparticles: Design, Synthesis, and Biomedical Applications *Acc. Chem. Res.*, **2009**, *42*, 1097–1107.

(29) Correa, D. N.; Silva, J. M. D. E.; Santos, E. B.; Sigoli, F. A.; Souza, A. G.; Mazali, I. O. TiO_2- and CeO_2-Based Biphasic Core–Shell Nanoparticles with Tunable Core Sizes and Shell Thicknesses. *J. Phys. Chem. C* **2011**, *115*, 10380-10387.

(30) Sutara, F.; Cabala, M.; Sedlacek, L.; Skala, T.; Skoda, M.; Matolin, V.; Prince, K. C.; Chab, V. Epitaxial growth of continuous CeO_2(111) ultra-thin films on Cu(111). *Thin Solid Films* **2008**, *516*, 6120-6124.

(31) Manea, F.; Houillon, F. B.; Pasquato, L.; Scrimin, P. Nanozymes: Gold-Nanoparticle-Based Transphosphorylation Catalysts. *Angew. Chem. Int. Edit.* **2004**, *43*, 6165-6169.

(32) Heckert, E. G.; Karakoti, A. S.; Seal, S.; Self, W. T. The role of cerium redox state in the SOD mimetic activity of nanoceria. *Biomaterials* **2008**, *29*, 2705-2709.

(33) Peng, Y. F.; Chen, X. J.; Yi, G. S.; Gao, Z. Q. Mechanism of the oxidation of organic dyes in the presence of nanoceria. *Chem. Commun.* **2011**, *47*, 2916-2918.

(34) Gao, L. Z.; Zhuang, J.; Nie, L.; Zhang, J. B.; Zhang, Y.; Gu, N.; Wang, T. H.; Feng, J.; Yang, D. J.; Perrett, S.; Yan, X. Intrinsic peroxidase-like activity of ferromagnetic nanoparticles. *Nat. Nanotechnol.* **2007**, *2*, 577-583.

(35) Chen, W.; Chen, J.; Liu, A. L.; Wang, L. M.; Li, G. W.; Lin, X. H. Peroxidase-Like Activity of Cupric Oxide Nanoparticle. *ChemCatChem* **2011**, *3*, 1151-1154.

(36) Dai, Z. H.; Liu, S. H.; Bao, J. C.; Jui, H. X. Nanostructured FeS as a Mimic Peroxidase for Biocatalysis and Biosensing. *Chem.-Eur. J.* **2009**, *15*, 4321-4326.

(37) Dutta, A. K.; Maji, S. K.; Srivastava, S. N.; Mondal, A.; Biswas, P.; Paul, P.; Adhikary, B. Synthesis of FeS and FeSe Nanoparticles from a Single Source Precursor: A Study of Their Photocatalytic Activity, Peroxidase-Like Behavior, and Electrochemical Sensing of H_2O_2 *ACS Appl. Mater. Interfaces,* **2012**, *4*, 1919–1927

(38) Song, Y. J.; Qu, K. G.; Zhao, C.; Ren, J. S.; Qu, X. J. Graphene Oxide: Intrinsic Peroxidase Catalytic Activity and Its Application to Glucose Detection. *Adv. Mater.* **2010**, *22*, 2206-2210.

(39) Reeder, A. E.; Agnoli, S.; Rizzi, G.; Granozzi, G. Zr_2O_3 Nanostripes on TiO_2(110) Prepared by UHV Chemical Vapor Deposition *J. Phys. Chem. C*, **2014**, *118*, 8026–8033

(40) Artiglia, L.; Agnoli, S.; Vittadini, A.; Verdini, A.; Cossaro A.; Floreano, L.; Granozzi, G.; Atomic Structure and Special Reactivity Toward Methanol Oxidation of Vanadia Nanoclusters on TiO_2(110) *J. Am. Chem. Soc.*, **2013**, *135*, 17331–17338.

(41) Ganduglia-Pirovano, M. V.; Popa, C.; Sauer, J.; Abbott, H.; Uhl, A.; Baron, M.; Stacchiola, D.; Bondarchuk, O.; Shaikhutdinov, S.; Freund, H. J. *J. Am. Chem. Soc.* **2010**, 132, 2345-2349.

(42) Chen, J.; Hu, P.; Brønsted–Evans–Polanyi Relation of Multistep Reactions and Volcano Curve in Heterogeneous Catalysis *J. Phys. Chem. C*, **2008**, *112*, 1308–1311.

(43) Lin, J.-L.; Wheeldon, I. Kinetic Enhancements in DNA–Enzyme Nanostructures Mimic the Sabatier Principle ACS Catal., **2013**, *3*, 560–564

GRAPHICAL ABSTRACT